Evaluation of Hydrogen Radical Production Using the Hydrogen Balmer-α Absorption Spectrum

Yuya INOKUCHI[1)]*, Kazutaka MITSUI[2)], Toshiro KASUYA[1)], Hidenori TAKAHASHI[2)], Yoshihiro YAMADA[2)], Takahiro KENMOTSU[1)], Shinichi IWAMOTO[2)], Koichi TANAKA[2)], Motoi WADA[1)]

[1)] *Doshisha University, Kyotanabe, Kyoto 610-0321, Japan*
[2)] *Shimadzu Corporation, Nakagyoku, Kyoto 604-8442, Japan*

(Received 13 May 2025 / Accepted 17 September 2025)

An ECR (Electron Cyclotron Resonance) discharge can serve as an efficient atomic hydrogen beam source for a bio-molecule mass analysis system through detecting fragment ions produced from the HAD (Hydrogen Attachment/Abstraction Dissociation) process. A simple diagnostics system that measures the absorption of photons from a light emitting diode located at the opposite side of the ECR plasma is coupled to a 4 mm inner diameter glass tube discharge source driven by a 2.45 GHz microwave. The obtained result for a fixed microwave input power shows a simple linear correlation between the duty cycle and the absorption indicating the production rate of atomic hydrogen is constant over the discharge duration. The dependence of absorption rate upon the discharge power and that upon pressure indicated that the efficiency of the atomic hydrogen production rate tend to saturate at higher power and higher pressure. The wavelength spectrum of Balmer-α light emission showed a possibility that high-speed atomic hydrogen may exist in an intense ECR discharge.

Keywords: optical emission spectroscopy, ECR plasma, atomic source, absorption spectroscopy

DOI: 10.1585/pfr.20.1406051

1. Introduction

Proteins that constitute biological tissues are synthesized by the transcription of the DNA base sequence into mRNA followed by the translation of mRNA into an amino acid sequence, which then gives functionality to the proteins. Synthesized proteins undergo changes in function and increase the diversity through the attachment of modifications called Post-Translational Modifications (PTM) [1]. For example, PTMs are known to play an important role in controlling cancer characteristics [2]. Quantum chemical calculations have also suggested a correlation between the patterns of PTM attachment and the incidence of Alzheimer's disease [3]. Understanding PTM binding is considered effective in cell biology and pathogenesis research. Mass spectrometry (MS) is an indispensable tool for protein analysis. Furthermore, tandem MS is widely used to analyze PTM binding, as it allows the analysis of PTM attachment patterns by mass spectrometry of fragmented molecules.

In tandem MS, the most common fragmentation technique is Collision-Induced Dissociation (CID) [4]. However, CID often preferentially dissociates thermally unstable PTM attachments, making PTM pattern analysis challenging. Therefore, there is a need for the development of alternative fragmentation techniques that can overcome the limitations of CID. Radical-induced fragmentation techniques, such as Electron Capture Dissociation (ECD) [5] and Electron Transfer Dissociation (ETD) [6], have shown effectiveness in determining PTM binding sites. However, sensitivities of these methods are limited by their reliance on electron-ion interactions, making them unsuitable for use with singly charged ions and severely limiting dissociation efficiency for lower charged ions, thereby imposing constraints on target molecules.

In 2016, Takahashi *et al.* at the Koichi Tanaka Mass Spectrometry Research Laboratory, Shimadzu Corporation introduced a new radical-induced fragmentation technique, known as the Hydrogen Attachment/Abstraction Dissociation (HAD) [7]. This technique allows for specific cleavage of peptide backbones while maintaining thermally unstable PTM attachments using low-energy hydrogen radicals in a mass spectrometer. The principle of the HAD was verified by generating hydrogen radicals using a thermal dissociation-type radical source at 2,000°C with a high-temperature tungsten capillary. The method produced high dissociation efficiency but accompanied high thermal radiation heating in the dissociation region, making it difficult to introduce reactive gas species like oxygen due to reactions with the hot metallic tungsten. In contrast, the ECR-LICP (Electron Cyclotron Resonance-Locally Inductively Coupled Plasma) radical source, which generates reactive radicals through discharge

*Corresponding author's e-mail: cygn0002@mail4.doshisha.ac.jp

[8], has been effectively applied in commercial systems for selective cleavage of fatty acid carbon double bonds using an oxygen radical induction method known as OAD (Oxygen Attachment Dissociation) [9].

Although it was initially considered easy to implement the HAD using the ECR-LICP hydrogen radical source, it was found that simply operating the ECR-LICP hydrogen radical source with hydrogen gas did not produce sufficient HAD reactions. Additionally, calculations by Asakawa *et al.* [10] revealed that only about 30% of the high-speed hydrogen radicals generated at 2,000°C in a thermal dissociation process contribute to the HAD cleavage reaction. This suggests that the velocity distribution function of hydrogen radicals generated by the ECR-LICP radical source lacks the high-speed components necessary for the HAD reaction. On the other hand, the newly developed radical source operation, which generates hydrogen plasma in a 4 mm inner diameter glass capillary in pulse mode, is expected to generate high-speed hydrogen radicals by operating at high power densities with low average power.

Therefore, this study aims to evaluate the velocity distribution function of hydrogen radicals emitted from the ECR-LICP hydrogen radical source using Doppler measurements of the Balmer-α spectral line of hydrogen atoms. Furthermore, the study attempts to find the possibility for investigating the production of high-speed hydrogen radicals based on spectroscopic measurements. A system was developed to evaluate the hydrogen atom production rate by adjusting instantaneous power while maintaining average power through pulse operation of the ECR-LICP hydrogen radical source. To evaluate the hydrogen radical production rate, LED light was irradiated onto the hydrogen plasma, and the absorption of the LED spectral intensity by hydrogen radicals was measured. Using this system, changes in absorption rate were studied by varying power and pressure, and the relative production rate of hydrogen radical was investigated.

2. Experimental Setup

This study employed a prototype atomic source used for research and development stages, rather than a commercially available plasma source for OAD [9]. The schematic structure of the ECR-LICP hydrogen radical source is shown in Fig. 1. Microwave power at 2.45 GHz induces electrical current to a coil antenna wound approximately 11 times around a glass tube with an outer diameter of 6 mm and an inner diameter of 4 mm, attached to an N-type connector. To ensure efficient power transmission, an impedance matching device such as a stub tuner is usually inserted between the connector and the coaxial transmission line. The ECR-LICP hydrogen radical source used in this study has an integrated impedance matching structure. Impedance matching is achieved by adjusting the length of the power application section by sliding a knob to change the position of the copper tube in contact with the grounded side of the copper coil antenna. Additionally, a forced air cooling is employed to prevent overheating

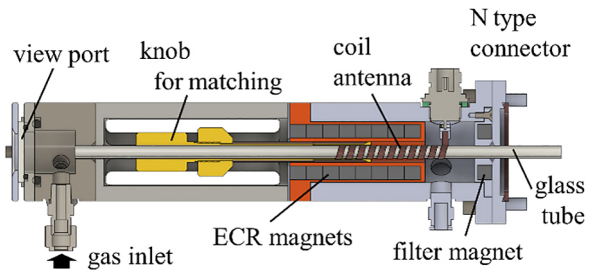

Fig. 1. A schematic diagram of the ECR-LICP type hydrogen radical source.

and degradation of the antenna by providing compressed air flow around the glass capillary tube. Magnets are placed inside the hydrogen radical source for ECR resonance. On the radical emission side, toroidal magnets are installed, and the charged particles of the produced plasma collide with the glass tube inside wall guided by the magnetic field lines of force, resulting in the emission of neutral radicals into the vacuum chamber.

For atomic emission spectrometry of hydrogen plasma, a monochromator (MC-100N model, Ritu Oyo Kougaku Co., Ltd.) with a resolution of 0.02 nm was used. Light passing through the entrance slit is reflected by mirrors and dispersed in wavelength by a diffraction grating. The light is then focused by another mirror and detected as a spectral signal by a CCD detector array. A diffraction grating with 1,200 grooves/mm from Richardson Gratings was used in this study. The CCD detector, the HAMAMATSU S7034-1007S image sensor (with 1,044 pixels), is equipped with a cooling function by a thermoelectric element. The element cools the image sensor to approximately −9°C during measurements. The entrance slit width and the CCD detector integration time were set to 30 μm and 100 ms, respectively.

The configuration of the lens focusing system used for absorption spectroscopy measurements is shown in Fig. 2. The optical bench is arranged along the spectrometer's line of sight, which extends from the radical emission side viewport to the gas inlet side viewport of the vacuum chamber with the ECR-LICP type hydrogen radical source installed. Light from the plasma is focused by a convex lens with a focal length of f_1 = 50 mm installed on the optical bench on the radical emission side and directed to a fiber optic cable. It then enters the monochromator through a 30 μm slit. On the gas inlet side, the optical bench is equipped with a red LED (Model: OSR7CA511P) with a peak wavelength of 660 nm and a convex lens with a focal length of f_2 = 60 mm. The emission spectrum of the LED is shown on Fig. 3. The LED is arranged so that the light passes through the glass tube of the radical source and the vacuum chamber to reach the focusing system on the radical emission side.

3. Method

Using the experimental setup shown in Fig. 2, the absorption rate of the spectrum emission of the LED at hydrogen

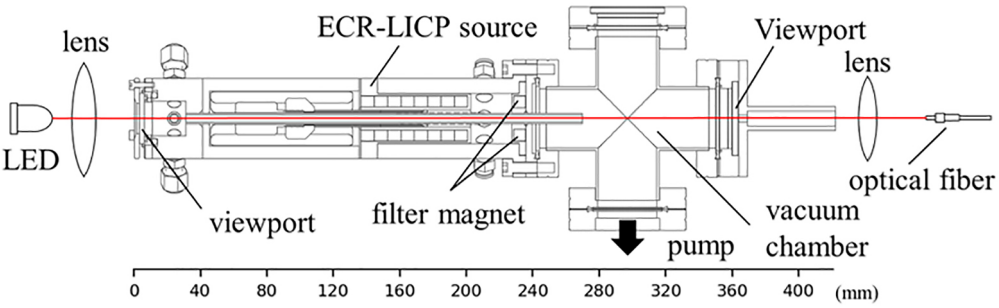

Fig. 2. Optical layout for the absorption spectrum measurement.

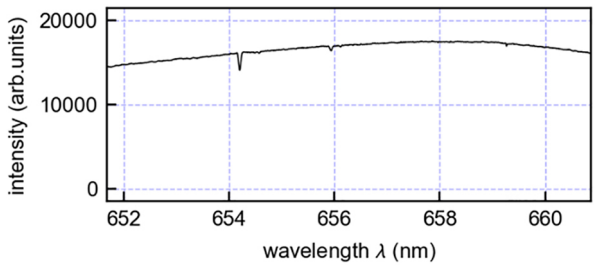

Fig. 3. The emission spectrum of the LED (Model: OSR7CA511P).

Balmer-α line wavelength after the passage of in the ECR-LICP hydrogen radical source was measured. The LED spectrum intensity, $I_{\mathrm{LED}}(\lambda)$, after the passage of the radical source exhibits the relationship against the light originates from the LED, $I_0(\lambda)$, following Lambert-Beer's law [11, 12]:

$$I_{\mathrm{LED}}(\lambda) = I_0(\lambda)\, e^{-k(\lambda)L}. \tag{1}$$

Here, $k(\lambda)$ is the product of the absorption coefficient at the wavelength and the absorption spectrum profile of hydrogen atoms, and L is the optical path of the high-density hydrogen atom volume.

However, the light absorbing hydrogen atoms originates from various locations within the plasma, making it difficult to define the optical path length L. In this study, it is assumed that there is no change of hydrogen atom density distribution by absorption of LED light. Therefore, $I_{p\mathrm{LED-ON}}$ the transmitted light intensity is equal to the original light intensity, $I_{p\mathrm{LED-OFF}}$; that is:

$$I_{p\mathrm{LED-ON}}(\lambda) \simeq I_{p\mathrm{LED-OFF}}(\lambda) \equiv I_p(\lambda). \tag{2}$$

The spectrum of the transmitted light, $I_t(\lambda)$, after passing through the hydrogen plasma and produced hydrogen radicals were measured. From Eqs. (1) and (2), $I_t(\lambda)$ is given by:

$$I_t(\lambda) = I_p(\lambda) + I_0(\lambda)\, e^{-k(\lambda)L}. \tag{3}$$

By subtracting the plasma light from the transmission light to obtain $(I_t - I_p)/I_0$, the absorption component with the term $e^{-k(\lambda)L}$ can be obtained. The plasma length along the optical axis is estimated to be approximately 10 cm based on the observation of emission pattern. However, hydrogen atoms are de-excited and recombined upon collisions at the glass tube wall surface making it difficult to determine the accurate optical path length L. Therefore, in this study, the absorption factor $e^{-k(\lambda)L}$ was obtained using Eq. (3), and the absorption rate α was derived.

The absorption rate α was determined based on the weighted average of the absorption factor $e^{-k(\lambda)L}$, as expressed by the following equation:

$$\alpha = 1 - \left\langle e^{-k(\lambda)L} \right\rangle = 1 - \frac{\int \left(I_t(\lambda) - I_p(\lambda)\right) \mathrm{d}\lambda}{\int I_0(\lambda) \mathrm{d}\lambda}. \tag{4}$$

This analysis allows investigation of the dependence of the absorption rate α on the microwave power supply operation conditions and hydrogen gas pressure for the ECR-LICP hydrogen radical source.

4. Result and Discussion

4.1 Duty cycle characteristics

In this study, to prevent overheating of the microwave transmission system and antenna, the ECR-LICP hydrogen radical source was operated using microwave power supply with pulse width modulation (PWM). The PWM frequency was fixed at 1 kHz, and the duty cycle, the ratio of the ON time to the total period of the gate pulse, was varied. The absorption rate α was measured under these conditions to evaluate the hydrogen atom production rate.

The hydrogen gas pressure downstream of the radical source was set to 4.5×10^{-2} Pa, and the instantaneous (on time) power was set to 250 W. The duty cycle was adjusted to 10, 20, and 30%, and the following spectra were measured: $I_p(\lambda)$ the hydrogen Balmer-α emission spectrum from plasma, $I_0(\lambda)$ the LED spectrum, and $I_t(\lambda)$ the sum of the LED spectrum obtained after the passage of the discharge and the light due to the plasma, as shown in Figs. 4(a) and (b). Focusing on the 0 to peak intensity of the emission spectra, the intensity of discharge + LED spectrum (Fig. 4(b)) was about 20% lower than that of plasma-only spectrum (Fig. 4(a)), indicating that the LED light was absorbed by the hydrogen atoms. The absorbed LED spectrum is calculated using Eq. (3) as $I_t(\lambda) - I_p(\lambda)$. Figure 5(a) shows the LED spectrum $I_t(\lambda) - I_p(\lambda)$ after being affected by the absorption near the hydrogen Balmer-α line, while Fig. 5(b) shows the original LED spectrum $I_0(\lambda)$ before the absorption.

The absorption rate of the spectral intensity was calculated from the simultaneous calculations of the three spectra by changing the duty cycle of the fixed microwave input

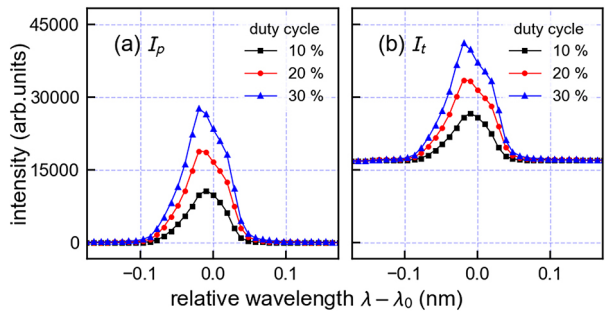

Fig. 4. Wavelength spectra around Balmer-α for (a): light emission from plasma, and (b): light emission from plasma and LED. Microwave power and downstream H_2 pressure are fixed at 250 W and 4.5×10^{-2} Pa, respectively.

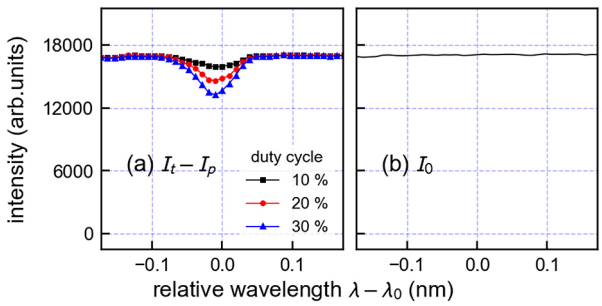

Fig. 5. Wavelength spectra around Balmer-α for (a): difference between the $I_t(\lambda)$ and $I_p(\lambda)$ spectra, and (b): light emission from LED. Microwave power and downstream H_2 pressure are fixed at 250 W and 4.5×10^{-2} Pa, respectively.

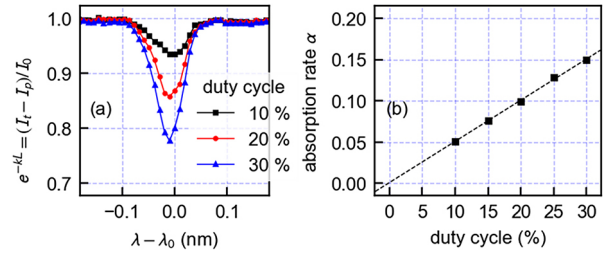

Fig. 6. (a): Change of absorption factor e^{-kL} for three different duty cycles: 10, 20 and 30%. (b): absorption rate α plotted as a function of duty cycle. Discharge power and downstream hydrogen pressure are fixed at 250 W and 4.5×10^{-2} Pa, respectively.

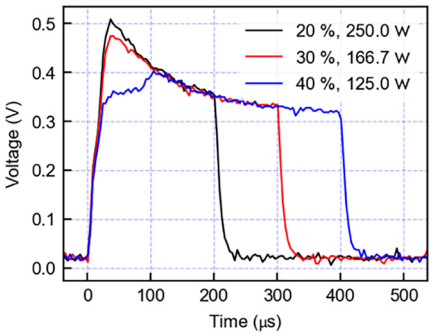

Fig. 7. Photo diode measurement of light emission from the plasma.

power. The measured duty cycle dependence of the absorption rate α was shown in Figs. 6(a) and (b) based on Eqs. (3) and (4). It was confirmed that the absorption rate α increased in proportion to the duty cycle. As the duty cycle increased, the pulse width also increased proportionally, extending the duration of hydrogen atom production. The observed proportional relationship between the duty cycle and the absorption rate can be expected if the hydrogen atom production rate keeps nearly constant during the pulse ON time.

For duty cycles of 10, 20, and 30%, and instantaneous powers of 250, 166.7, and 125 W, the plasma emission intensity was measured with a photodiode from the viewport on the gas inlet side. The results are shown in Fig. 7. The plasma light emission intensity right after the discharge ignition reached the similar peak height. After the peak, the emission intensity gradually decayed converging to the same final waveform in a time duration of several hundred microseconds. In other words, except for the initial discharge rise, stable plasma light emission is maintained during the pulse ON time for each duty cycle, and the hydrogen atom production rate seems nearly constant within the pulse duration. From this observation, it is inferred that the increase in absorption rate proportional to the duty cycle, as shown in Fig. 6(b), is due to the constant hydrogen atom production during the pulse time. Additionally, the initial emission intensity peak decreases with the decrease in instantaneous power as shown in Fig. 7. This initial light emission characteristic will be discussed in the next section relating the effect to instantaneous power changes on the hydrogen atom absorption rate.

4.2 Microwave power characteristics

The hydrogen gas pressure downstream of the atomic source was set to 4.5×10^{-2} Pa, the duty cycle was set to 20%, and the instantaneous power was varied at 30, 80, and 250 W. The absorption rates of the spectral intensity for these input powers are shown in Fig. 8(a). As the power increased, the absorption intensity also increased, suggesting an increase in hydrogen atom production rate. Additionally, a tendency was observed that the emission peak of the absorption spectrum shifted to shorter wavelengths with increasing power. This shift may be attributed to the Doppler effect caused by the production of high-speed hydrogen atoms due to the increase in discharge power. In Fig. 8(b), the instantaneous power dependence of the absorption rate α, calculated based on Eq. (4), is shown. The absorption rate α tends to increase in proportion to the microwave input power, while a change in the proportional constant against the power increase near an instantaneous power around 60 W was observed. This change can be due to the transition from the low-density discharge mode, or E-mode (electrostatic), to the high-density discharge mode, or H-mode (electromagnetic) inductively coupled plasma (ICP). In E-mode discharge, plasma is maintained mainly by capacitive coupling via the local electric field between plasma and coil antennas, whereas in H-mode, plasma is maintained by inductive coupling

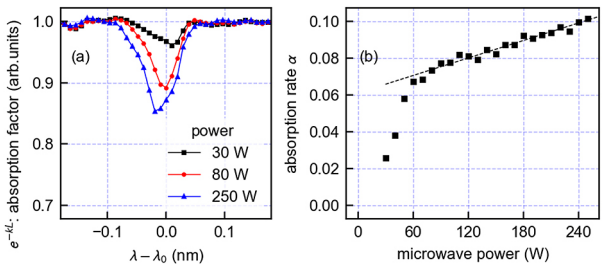

Fig. 8. (a): Change of absorption factor e^{-kL} for different input microwave power. (b): absorption rate α of Balmer-α plotted as a function of microwave power. Downstream hydrogen pressure and duty factor are fixed at 4.5 × 10^{-2} Pa and 20%, respectively.

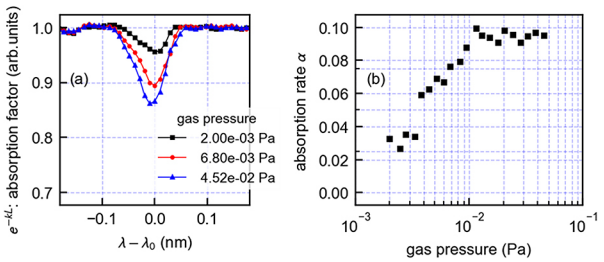

Fig. 9. (a): Change of absorption factor e^{-kL} due to increase in hydrogen gas pressure. (b): absorption rate α plotted as a function of downstream hydrogen gas pressure. Microwave power and duty factor are fixed at 250 W and 20%, respectively.

through the induced electromagnetic field from the microwave power applied to the coil antenna. In H-mode, higher electron density and ionization efficiency are realized compared to E-mode, resulting in higher hydrogen atom production efficiency and thus, an enhancement in the absorption rate α. The existence of such mode transitions in ECR-LICP-type radical sources has been shown as a jump in emission intensity by Shimabukuro *et al.* [8] Linear correlation between emission intensity and instantaneous power has been confirmed in the same reference. As shown in Fig. 8(b), the linear relationship between absorption rate α and instantaneous power in the ECR-LICP-type hydrogen radical source used in this study indicates a linear correlation between emission intensity and hydrogen atom production.

4.3 Hydrogen gas pressure characteristics

To evaluate the hydrogen gas pressure dependence of the absorption rate, the duty cycle was set to 20%, and the instantaneous power was fixed at 250 W. The hydrogen gas pressure was maintained at 2.0 × 10^{-3}, 6.8 × 10^{-3}, and 4.5 × 10^{-2} Pa. The measured absorption rates of the spectral intensity are shown in Fig. 9(a). With the increase in hydrogen gas pressure, the absorption rate increased, and a shift of the spectrum to shorter wavelengths was also observed. The hydrogen gas pressure dependence of the absorption rate α, calculated based on Eq. (4), is shown in Fig. 9(b).

In the range up to approximately 10^{-2} Pa, the absorption rate increased with gas pressure. Above 10^{-2} Pa downstream pressure α tends to take a constant value around 10%. The absorption rate α is determined by the line integral of the excited hydrogen atom density at the n = 2 energy level where n is the principal quantum number. The excited atom density is determined by the balance between the production of excited atoms due to collisions between hydrogen molecules and electrons, and de-excitation of produced excited atoms. If the de-excitation rate for the excited atoms is dominated by processes independent upon the hydrogen molecular density, such as de-excitation at the discharge tube wall, the excited atoms increase with the increasing rate of excitation proportional to pressure. The balance between the excitation and de-excitation rate should cause constant excited atom density at higher pressure when the de-excitation rate also becomes proportional to the hydrogen molecule density in the discharge tube.

5. Summary and Outlook

By measuring the absorption rate using the hydrogen Balmer-α spectrum, it was confirmed that the absorption rate increased in proportion to the duty cycle of the microwave input power. Additionally, the photodiode-based light emission intensity measurement demonstrated that the hydrogen atom production rate remains nearly constant during the pulse ON time under the measurement condition. As the instantaneous power increased, the absorption rate of Balmer-α also increased. In the input power region above 60 W, a change was observed where the increase in absorption rate corresponded to the rise in emission intensity due to the discharge mode transition. On the other hand, the dependence of absorption rate upon the downstream hydrogen gas pressure indicated that the absorption rate increased with the gas pressure below 10^{-2} Pa. However, in the pressure range above 10^{-2} Pa, the absorption rate tended to saturate.

From these results, it is considered that for efficient hydrogen atom production with a duty cycle of 20%, the microwave power should be between 70–90 W, and the downstream hydrogen gas pressure should be kept about 1 × 10^{-2} Pa. Beyond these power and pressure levels, the hydrogen atom production rate is unlikely to improve significantly.

The wavelength spectra shown in Fig. 4 can indicate a small shift of the peak wavelength (about 0.02 nm) with the increase from 10 to 30% duty cycle. The transition state barrier for the hydrogen radical attachment to the carbonyl oxygen in the peptide has been reported to range from 38 to 68 kJ/mol [13] corresponding to 0.019 nm minimum shift at the Balmer-α wavelength. With the spectrometer resolution of 0.02 nm, the linear image sensor monitors light intensity in every 0.01 nm in the current setting. Thus, an evaluation of the high-speed component of plasma produced hydrogen atom may be possible with the present set up but with some more tuning of the optical system that occasionally exhibits change of the spectral shape possibly attributable to the spatial distribution of the plasma.

In conclusion, the effectiveness of pulse operation of a

small, high-power density hydrogen radical source can be evaluated by Balmer-α absorption spectroscopy. It was found that by reducing the duty cycle, the average input power can be lowered, and by increasing the instantaneous input power, hydrogen atoms with high-speed components can be generated. Future work will focus on further development of the measurement system and establishing a highly reliable system for monitoring the performance of the hydrogen radical source.

Acknowledgements

This work was supported by JSPS KAKENHI Grant Number 23K25855.

[1] G. Grotenbreg and H. Ploegh, Nature **446**, 994 (2007).
[2] H. Wang *et al.*, Cancer Gene. Ther. **30**, 529 (2023).
[3] H. Wesseling *et al.*, Cell **183**, 1699.e13 (2020).
[4] S.A. McLuckey, J. Am. Soc. Mass Spectrom. **3**, 599 (1992).
[5] R.A. Zubarev *et al.*, J. Am. Chem. Soc. **120**, 3265 (1998).
[6] J.E.P. Syka *et al.*, Proc. Natl. Acad. Sci. **101**, 9528 (2004).
[7] H. Takahashi *et al.*, Anal. Chem. **88**, 3810 (2016).
[8] Y. Shimabukuro *et al.*, Plasma Sources Sci. Technol. **29**, 015005 (2020).
[9] H. Takahashi *et al.*, Anal. Chem. **90**, 7230 (2018).
[10] D. Asakawa *et al.*, J. Am. Soc. Mass Spectrom. **31**, 450 (2020).
[11] A.C.G. Mitchell and M.W. Zemansky, *Resonance Radiation and Excited Atoms* (Cambridge University Press, Cambridge, England, 1961), 92–93.
[12] K. Takeda *et al.*, J. Plasma Fusion Res. **95**, 180 (2019) [in Japanese].
[13] F. Tureček and R.R. Julian, Chem. Rev. **113**, 6691 (2013).